Supplementary Information

Integrated microfluidic device for rapid and accurate point-of-care detection of high-risk HPV16 and HPV18

Natish kumar, [a,] Monika Kumari, [a,] Devtulya Chander, [b,] Sandeep Dogra,[c,] Asha Chaubey,[b,] Ravi Kumar Arun, [a,]

[a]Department of Chemical Engineering, Indian Institute of Technology, Jammu, 181221, India

[b]Fermentation and Microbial Biotechnology Division, CSIR-Indian Institute of Integrative Medicine, Canal Road, Jammu-180001, India

[c]Department of Microbiology, Govt. Medical College, Jammu, 180001, India

[*]Corresponding Author- ravi.arun@iitjammu.ac.in

Contents

Supplementary Figure S8. Off-cartridge qPCR reference assay demonstrating the inverse relationship between Ct values and input DNA copies/µL for HPV-16 and HPV-18 targets.

Supplementary Figure S9. Semi-quantitative on-cartridge LAMP analysis showing linear relationships between threshold amplification time and DNA copies/µL for HPV-16, HPV-18, and β-actin targets.

Supplementary Figure S10. Specificity assessment of LAMP primer sets confirming target-specific amplification for β-actin, HPV-16, and HPV-18 with no cross-reactivity toward non-target HPV templates.

Supplementary Figure S11. ImageJ-based quantitative analysis workflow for lateral flow signal extraction using defined regions of interest.

Table S1. Primer Sequences for HPV-16 E6, HPV-18 E6, gene and Human β-Actin Gene

Table S2. LAMP + lysis + LFA consumables (per test)

Table S3. Cartridge raw materials (example costing)

Table S4. One-time device cost (heater + controller + sensor + PSU)

Table S5. Comparison of HPV Detection Technologies (HPV16/18)

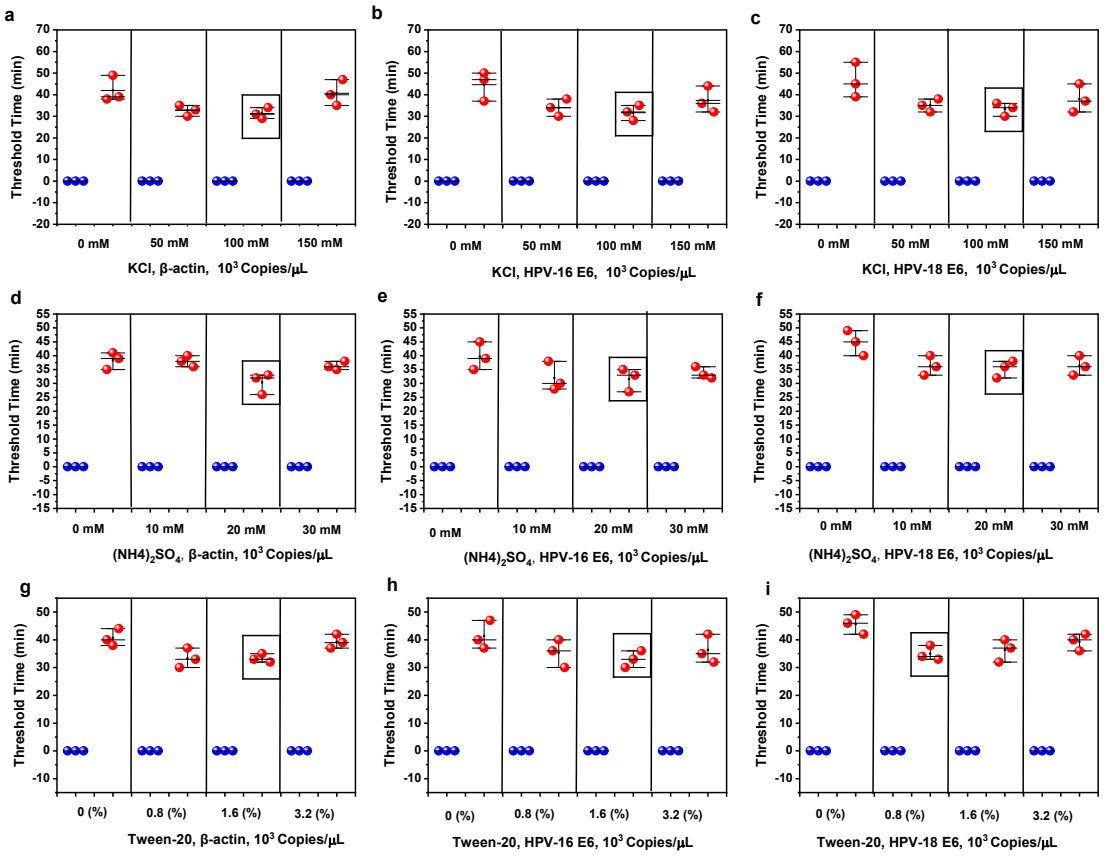

Fig. S1. Optimization of LAMP reaction buffer components for amplification of the β-actin housekeeping gene and high-risk HPV targets. Scatter plots show the effect of varying concentrations of KCl (a–c), ammonium sulfate $(NH_4)_2SO_4$ (d–f), and Tween-20 (g–i) on LAMP amplification performance for β-actin (a, d, g), HPV-16 E6 (b, e, h), and HPV-18 E6 (c, f, i) targets. Positive controls (red circles) containing 1,000 copies μL^{-1} of target DNA and no-template negative controls (blue circles) were measured in triplicate (n = 3) for each condition. Individual data points are shown, with error bars representing the mean ± standard deviation. The optimal concentration of each buffer component, selected based on maximal amplification efficiency and minimal nonspecific background, is indicated by a black square. These optimized conditions were used for subsequent on-cartridge LAMP experiments.

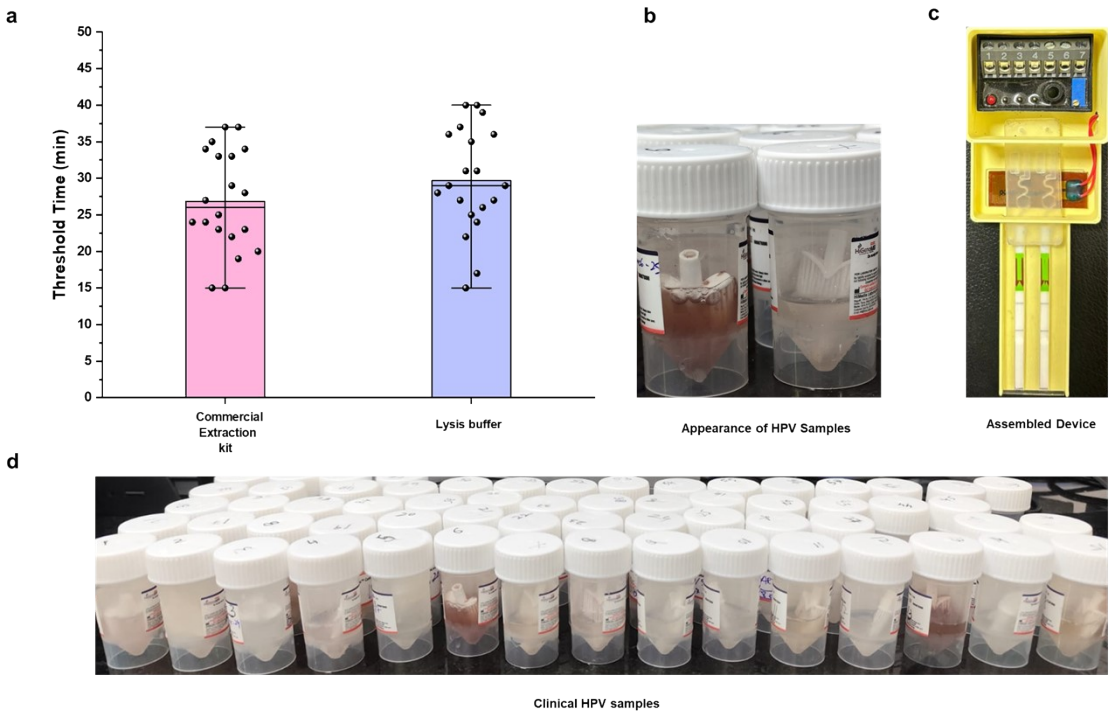

Fig. S2 Clinical sample collection, lysis, and on-cartridge processing for extraction-free HPV detection. (a) Lysis efficiency of the optimized extraction-free buffer in clinical cervical swab samples, demonstrating effective disruption of cellular material and release of nucleic acids. (b) Representative appearance of HPV-positive clinical samples immediately after collection in Viral Transport Medium (VTM) and following lysis treatment. (c) Photograph of the integrated microfluidic device used for on-cartridge processing and amplification, incorporating the heating module and cartridge holder for controlled LAMP reactions. (d) A batch of collected clinical cervical swab samples was prepared for on-cartridge analysis, illustrating the scalability, uniformity, and consistency of the sample handling workflow prior to testing.

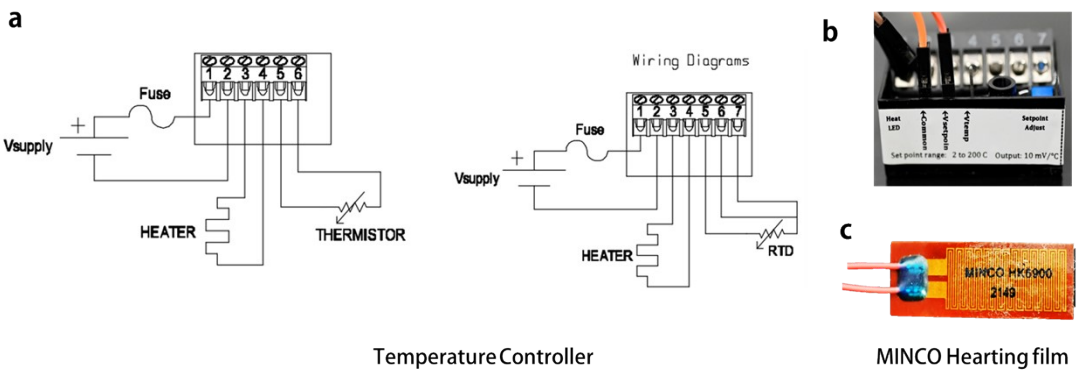

Fig. S3. Schematic representation and components of the temperature control system: (a) Circuit diagram showing the basic wiring and connections for thermal regulation; (b) Digital temperature controller (CT325) responsible for monitoring and maintaining the set temperature; (c) Flexible film heater (MINCO HK69002149, 10 mm × 30 mm) used to uniformly heat the amplification zone from both top and bottom sides.

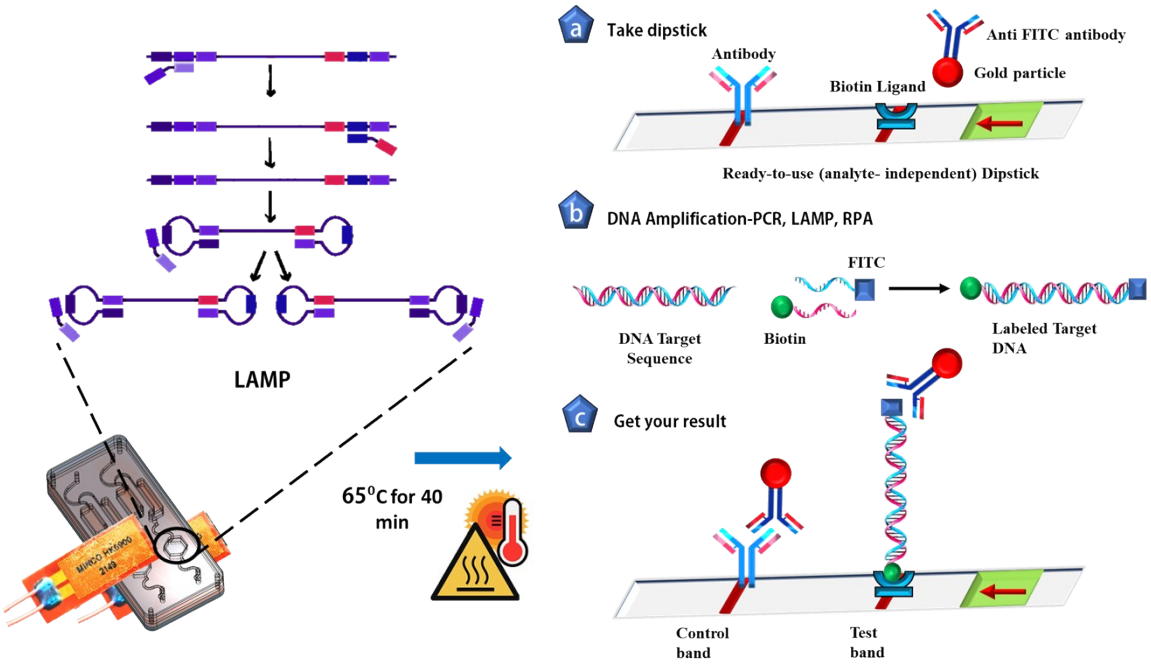

Fig. S4. Schematic of the integrated microfluidic system for HPV-16 and HPV-18 DNA detection. The system performs on-chip isothermal amplification using a LAMP reaction at 65°C, facilitated by a compact heating module. Labelled amplicons are then directed to an integrated lateral flow strip, where genotype-specific capture lines enable visual identification of HPV-16 and HPV-18 within 60 minutes. The closed, portable design supports contamination-free, point-of-care diagnostics.

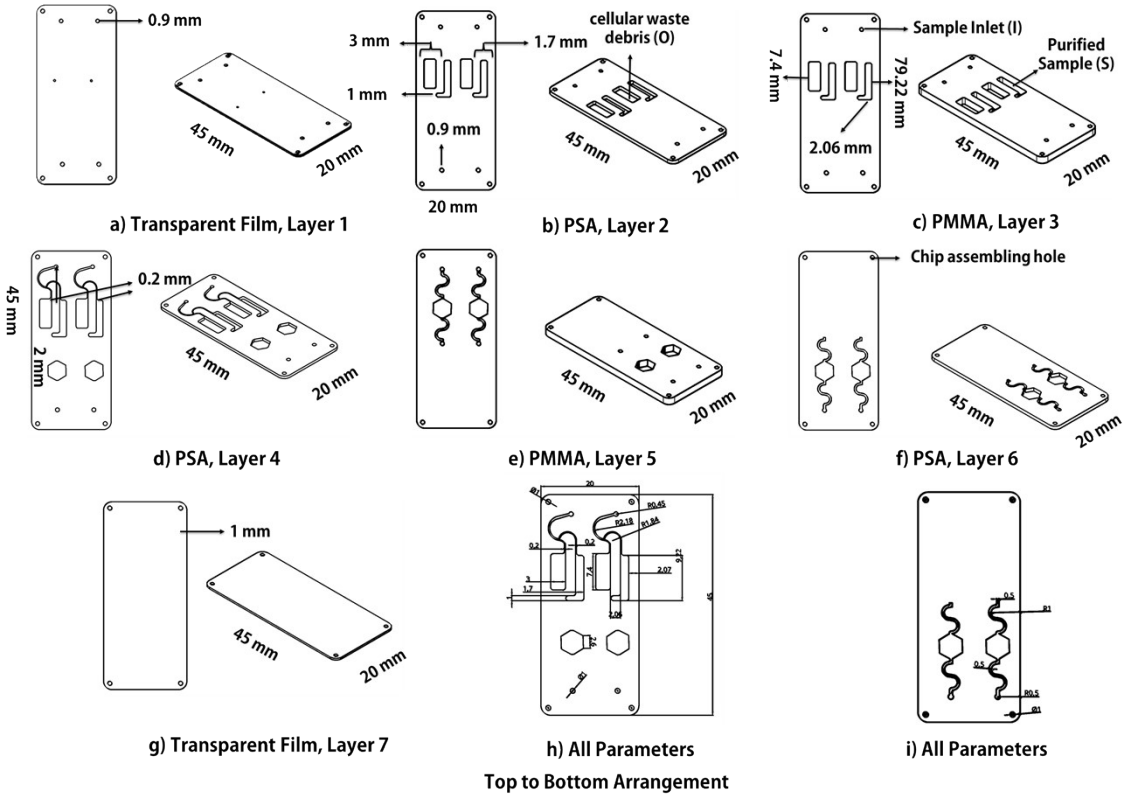

Fig. S5. Schematic layout and dimensions of the fabricated microfluidic cartridge. (a-i) The figure displays the top-to-bottom layer arrangement and highlights the key functional zones, including the sample inlet (I), a separation channel for cellular debris (O), and a dedicated chamber for purified nucleic acid collection (S). Each section is annotated with precise dimensions, illustrating the structural design necessary for efficient fluid routing, waste removal, and nucleic acid isolation within the compact cartridge footprint.

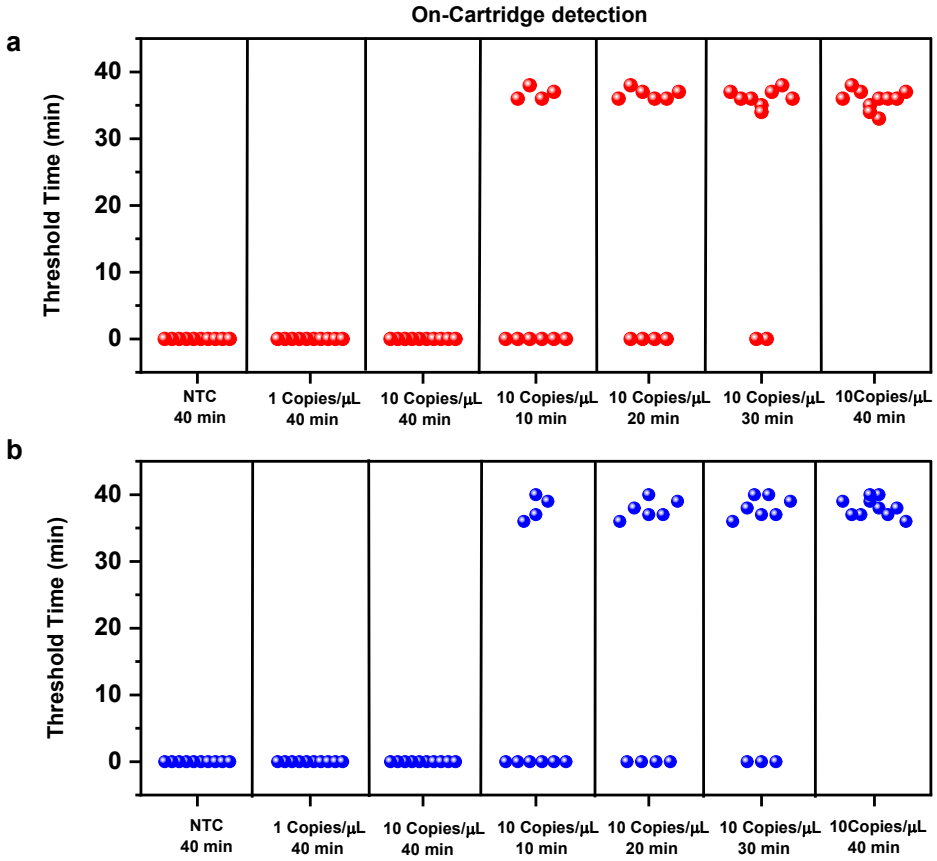

Fig. S6. Time-dependent on-cartridge detection performance of the integrated LAMP–LFA platform for high-risk HPV genotypes. Red data points represent HPV-16–positive samples, and blue data points represent HPV-18–positive samples. Ten no-template controls (NTCs) and low-copy target samples (1 copy and 10 copies μL^{-1}) were evaluated at different amplification times (10, 20, 30, and 40 min). For HPV-16 at 10 copies μL^{-1}, positive detection was observed in 4 out of 10 samples after 10 min, 6 samples after 20 min, 8 samples after 30 min, and all samples after 40 min of amplification. In contrast, HPV-18 samples achieved 100% positive detection after 40 min. These results demonstrate a clear time-dependent increase in detection efficiency, establishing 40 minutes as the optimal amplification time for reliable on-cartridge LAMP detection of both HPV-16 and HPV-18.

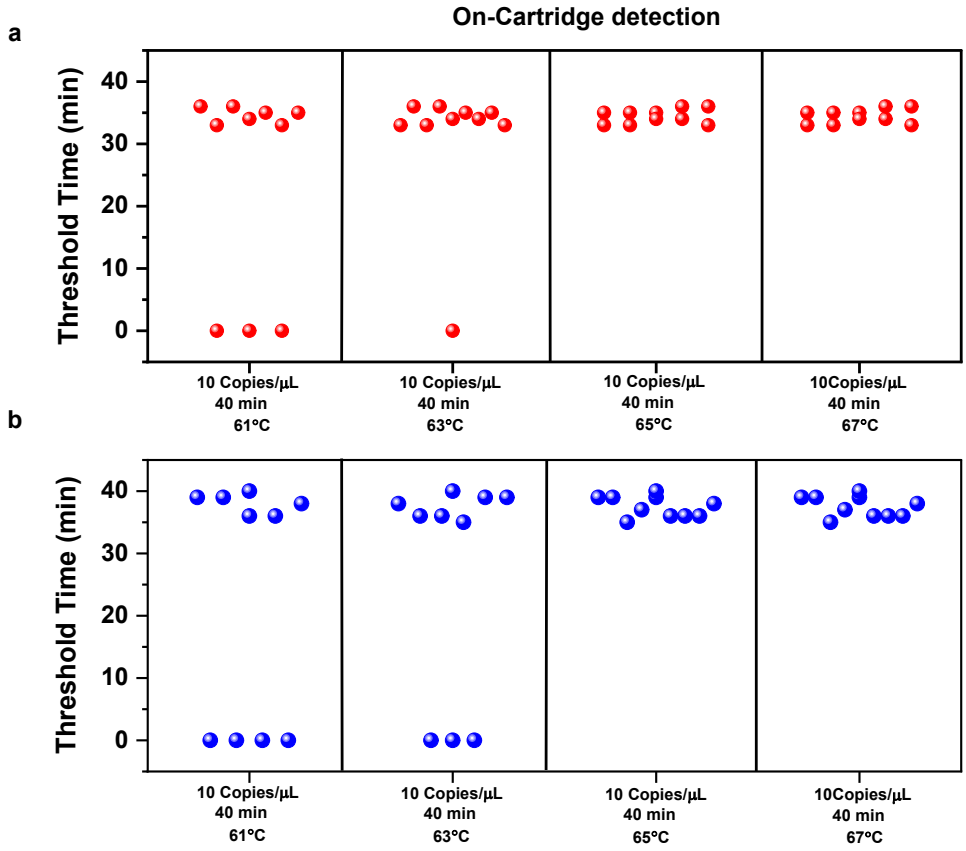

Fig. S7 Temperature-dependent on-cartridge detection performance of the integrated LAMP–LFA platform for high-risk HPV genotypes. Red data points correspond to HPV-16–positive samples, while blue data points represent HPV-18–positive samples. Ten samples were tested on a single cartridge at different heating chip temperatures (61, 63, 65, and 67 °C). For HPV-16, positive detection was observed in 6 out of 10 samples at 61 °C, 9 out of 10 samples at 63 °C, and in all 10 samples at both 65 °C and 67 °C. For HPV-18, 6 out of 10 samples were positive at 61 °C, 7 out of 10 samples at 63 °C, and all samples were positive at 65 °C and 67 °C. These results demonstrate a clear temperature-dependent increase in amplification efficiency, establishing 65 °C as the optimal temperature for reliable on-cartridge LAMP detection of both HPV-16 and HPV-18.

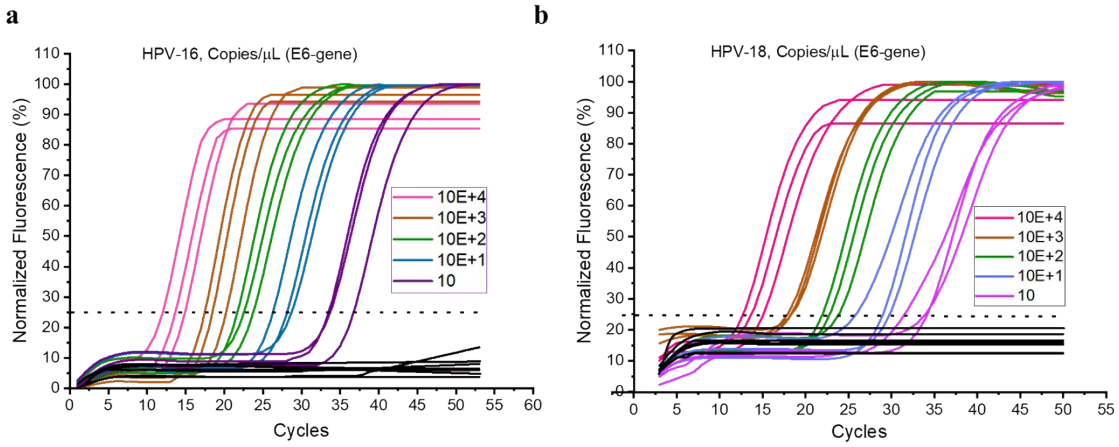

Fig. S8 Analytical characterization of the off-cartridge real-time PCR (qPCR) assay used as a reference method for HPV detection. Normalized fluorescence amplification curves are shown for serially spiked control DNA copies/µL targeting (a) the HPV-16 E6 gene and (b) the HPV-18 E6 gene. Samples containing higher DNA copies/µL exhibited earlier amplification and lower cycle threshold (Ct) values, reaching the fluorescence threshold in fewer PCR cycles, whereas lower copies/µL required more cycles to reach the threshold. These results confirm the expected inverse relationship between the Ct value and initial DNA concentration, validating the qPCR assay as a quantitative benchmark for comparison with the on-cartridge LAMP platform.

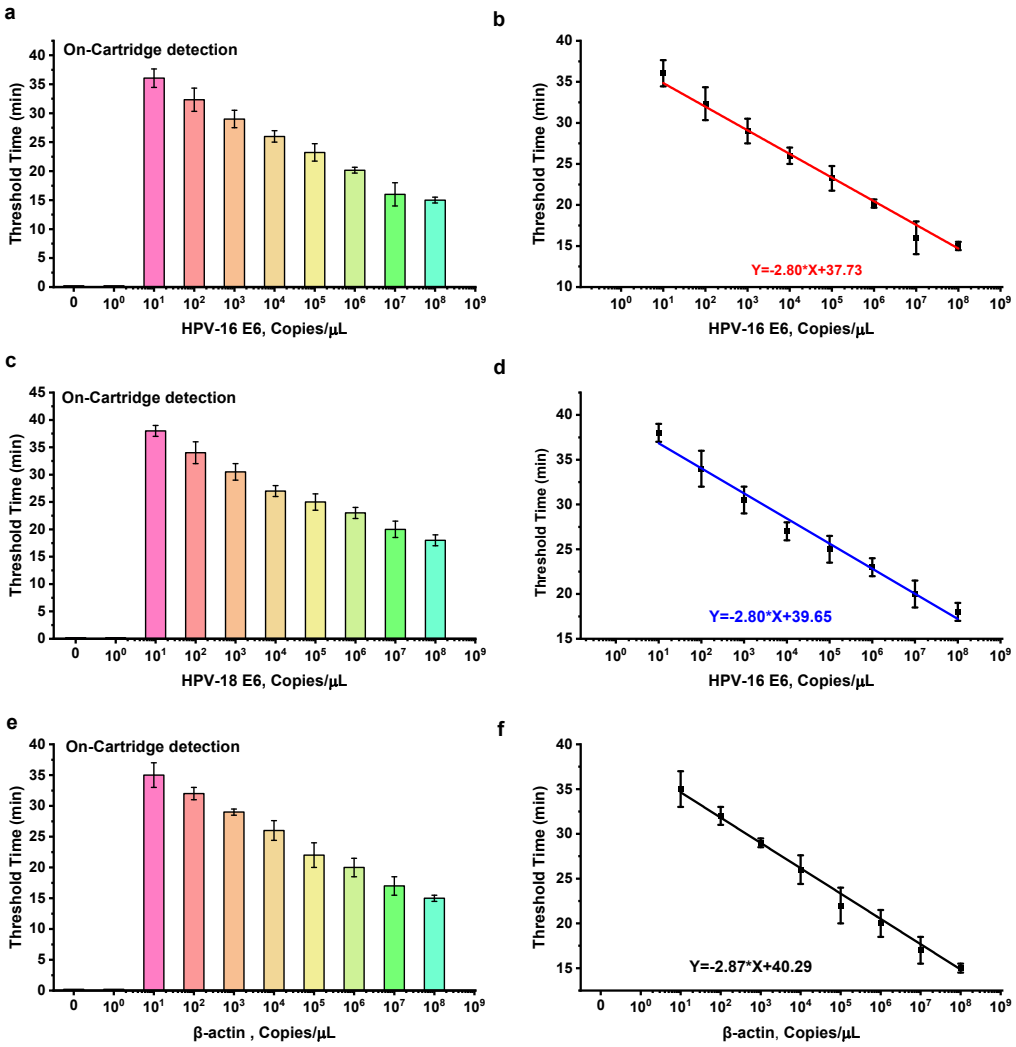

Fig. S9 Semi-quantitative characterization of on-cartridge LAMP amplification kinetics for HPV and internal control gene targets. (a) Threshold amplification times measured for serially spiked DNA copies/µL targeting the HPV-16 E6 gene, showing a progressive decrease in threshold time with increasing template concentration. (b) Calibration plot correlating threshold amplification time with the logarithm of HPV-16 E6 DNA copies/µL , exhibiting a strong linear relationship described by Y = −2.80X + 37.73. (c) Corresponding threshold amplification time data for the HPV-18 E6 gene, demonstrating a similar concentration-dependent trend. (d) Threshold time versus log DNA copies/µL calibration plot for HPV-18 E6, following the linear equation Y = −2.80X + 39.65. (e) Threshold amplification time analysis for the β-actin housekeeping gene under identical on-cartridge reaction conditions, confirming consistent amplification kinetics across targets. (f) Calibration plot of threshold amplification time versus log DNA copies/µL for β-actin, described by the linear equation Y = −2.80X + 40.29. Error bars represent the standard deviation of three independent experiments. Collectively, these results demonstrate a linear decrease in threshold amplification time with increasing DNA copies/µL across HPV and internal control gene targets, supporting the semi-quantitative capability and reproducibility of the integrated microfluidic LAMP platform.

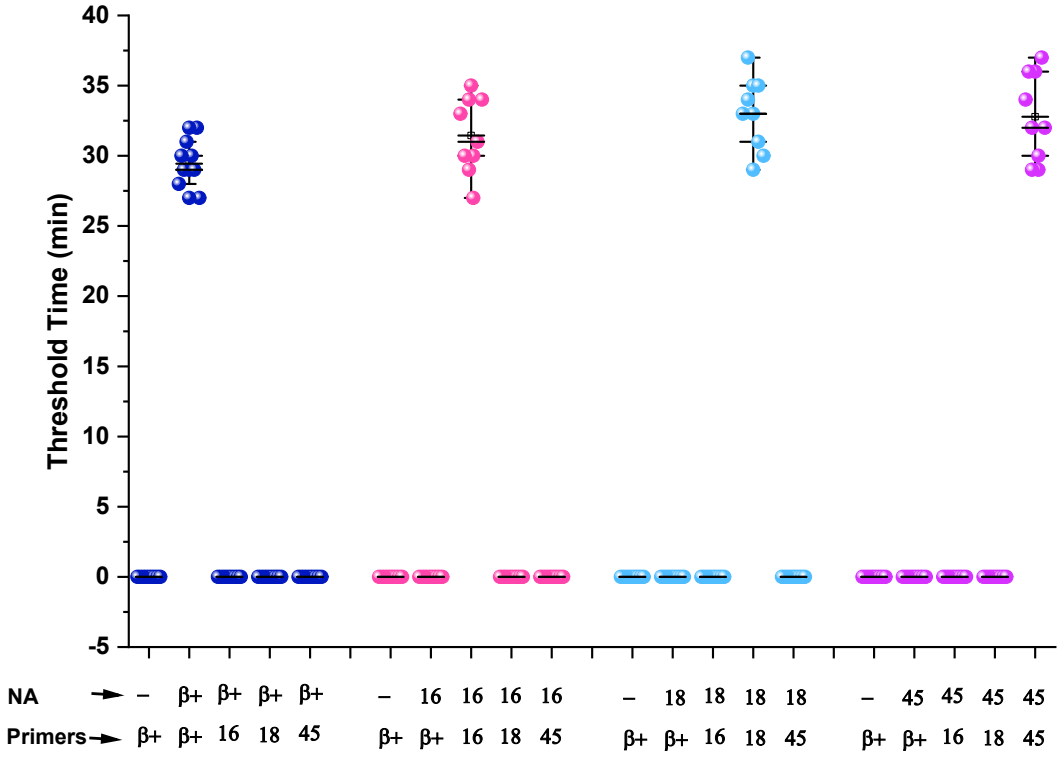

Fig. S10 Specificity evaluation of LAMP primer sets for β-actin, HPV-16, HPV-18, and HPV-45 using 1,000 copies of target and non-target nucleic acid templates to assess cross-reactivity. Data points are color-coded according to the nucleic acid template used: purple represents β-actin DNA, magenta represents HPV-16 DNA, cyan represents HPV-18 DNA, and light magenta rose represents HPV-45 DNA. The x-axis denotes different primer–template combinations tested to assess assay specificity. The first column corresponds to β-actin primers with no-template control (NTC), the second column shows β-actin primers with β-actin–positive DNA, the third column represents β-actin–positive DNA tested with HPV-16 primers, the fourth column shows β-actin–positive DNA tested with HPV-18 primers, and the fifth column represents β-actin–positive DNA tested with HPV-45 primers. Similarly, HPV-16 and HPV-18 primer sets were tested against their respective target DNAs as well as non-target HPV templates. Specific amplification was observed only when each primer set was paired with its corresponding target nucleic acid, while no cross-reactivity or nonspecific amplification was detected with non-target templates. These results confirm the high specificity of the β-actin, HPV-16, and HPV-18 LAMP primer sets.

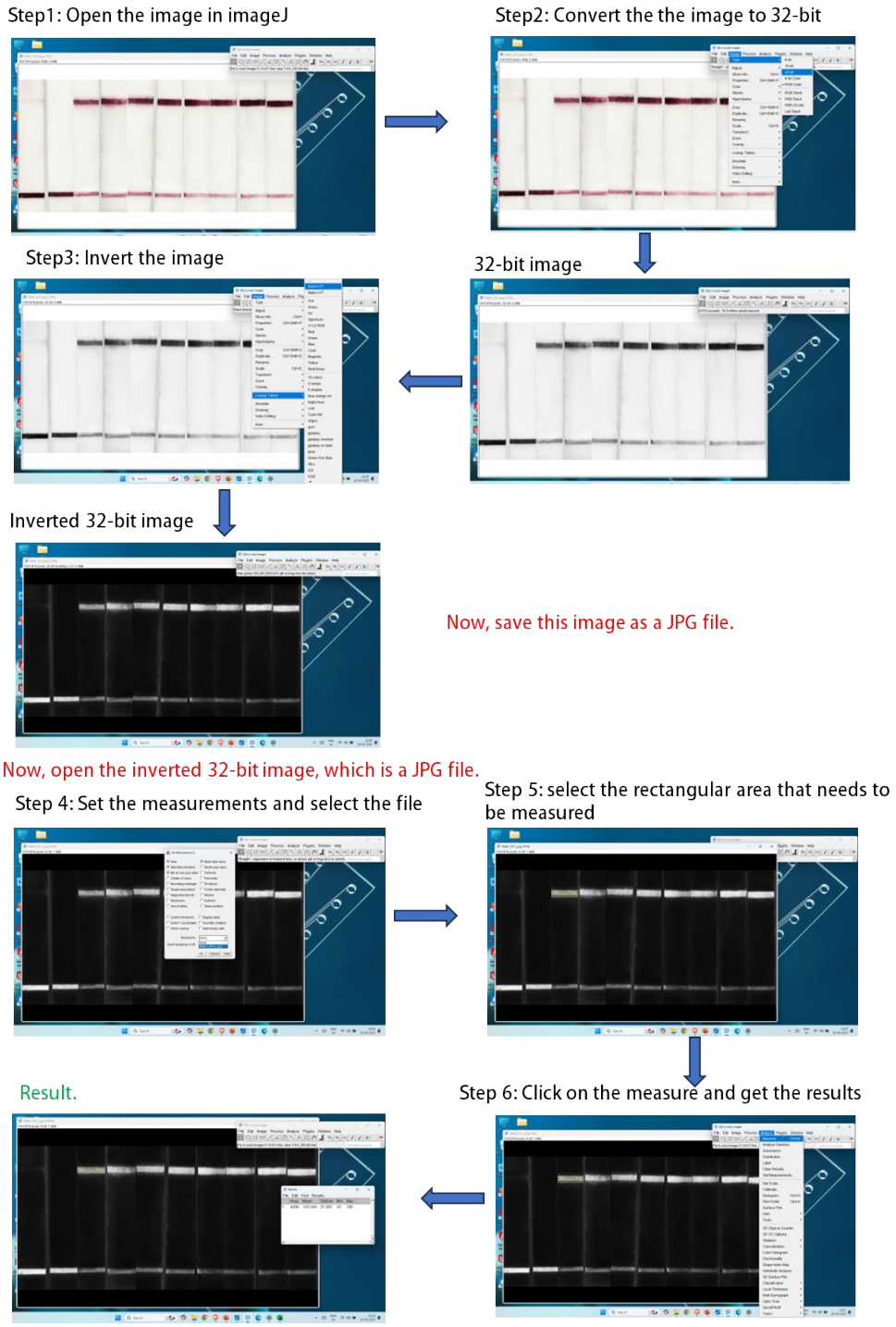

Fig. S11 Quantitative image analysis using ImageJ. The original image was converted to a 32-bit format and subsequently inverted to enhance contrast. The processed image was saved in JPG format and reloaded for analysis. A specific rectangular region of interest (ROI) was selected, and measurements were obtained using ImageJ's measurement tool after setting the desired parameters.

Table S1. Primer Sequences for HPV-16 E6 and E7, HPV-18 E6 and E1 gene, HPV-45L1 and Human β-Actin Gene

HPV-16-E7 Sequences		
Label	**Length**	**Sequence 5'-3'**
16 e7F3	19	AACAAACCGTTGTGTGATT
16 e7B3	8	TCAGTTGTCTCTGGTTGC
16 e7FIP	47	ATCTTTGCTTTTTGTCCAGATGTCTGTGTATTAACTGTCAAAAGCCA
16 e7BIP	5	BIOTIN-GGTCGATGTATGTCTTGTTGCAGACAATGTAGGTGTATCTCCATG
16 e7LB	5	FITC PROBE-TCAAGAACACGTAGAGAAACCCAGC
HPV-16-E6 Sequences		
16 e6F3	19	ATGCACCAAAAGAGAACTG
16 e6B3	20	AGCATATGGATTCCCATCTC
16 e6FIP	39	BIOTIN-GCAGCTCTGTGCATAACTGTCAATGTTTCAGGACCCACA
16 e6BIP	41	AGAATGTGTGTACTGCAAGCAATCCCGAAAAGCAAAGTCAT
16e6LF	21	GGTAACTTTCTGGGTCGCTCC
16e6LB	20	CAGTTACTGCGACGTGAGGT
16 e6FITC-PROBE	23	AACAACTATACATGATATAATAT
HPV-18-E6 Sequences		
18 e6F3	23	AAAAACTAACTAACACTGGGTTA
18e6B3	18	ACTTGTGTTTCTCTGCGT
18 e6FIP	47	GGTGTCTAAGTTTTTCTGCTGGATAATTTATTAATAAGGTGCCTGCG
18 e6BIP	41	BIOTIN-CGACGATTTCACAACATAGCTGG-GTTGGAGTCGTTCCTGTC
18 e6LB	21	FITC-CATTCGTGCTGCAACCGAGCA
HPV-18-E1 Sequences		
18 e1F3	19	CAGGGTCGGATATGGTAGA
18 e1B3	18	TTGCCTTTTTCTGCCCAC
18 e1FIP	42	CATCATTGTGGACCTCCTGCG-CACAAGGAACATTTTGTGAAC
18 e1BIP	39	BIOTIN-CGAAAGTTTGCAGGAGGCAGAACCGTGGACTTAACTCTG
18 e1LF	19	FITC-GCTGTCTCTAGCTCTGCCT
18 e1LB	23	CACAGAAAACAGTCCATTAGGGG
HPV-45-L1 Sequence		
45 L1F3	23	GGCCATGGTATTATTATTTTCCT

45 L1B3	**23**	**CCTAAAATATGGATTGCCTACAG**
45 L1FIP	**41**	**ACCGTACTGTCACTAGGCCG-AAAAACGTAAACGTATTCCCT**
45 L1BIP	**43**	**ATCTTCCACCACCTTCTGTGG-TGCATGATAAAATATGCTTGTG**
45 L1LF	**22**	**CCACAAAGCCATCTGCAAAAAA**
45 L1LB	**21**	**CCAGAGTTGTCAGCACTGATG**
Human β-actin reference genome sequence (NM_001101.5)		
act1F3	**19**	**GGCATCCTCACCCTGAAGT**
act1B3	**20**	**TGGGGTGTTGAAGGTCTCAA**
act1FIP	**41**	**Biotin-GCCACACGCAGCTCATTGTAGA-CATCGAGCACGGCATCGTC**
act1BIP	**38**	**AGCACCCCGTGCTGCTGA-GGTCATCTTCTCGCGGTTGG**
act1LF	**22**	**FITC- TCTCCATGTCGTCCCAGTTGGT**

Table S1 outlines the genomic coordinates, region lengths, and nucleotide sequences of the primers designed for amplifying the E6 gene (associated with HPV-16 and HPV-18) and the human β-actin gene, which serves as an internal control. This comprehensive dataset ensures precise targeting and efficient amplification for downstream molecular assays, such as LAMP, in HPV detection workflows.

Table S2. LAMP + lysis + LFA consumables (per test)

Module	Component (example supplier)	Pack price (currency)	Pack size	Assumed use per test	Cost per test (USD)
LAMP	Bst 3.0 DNA polymerase (NEB list price)	$343.00	8000 U	8 U	0.34
LAMP	Isothermal Amplification Buffer II (10X)	$32.00–$33.00	6 mL	3.5 µL	0.02
LAMP	dNTP mix 10 mM each Thermo Fisher Scientific	$132.65	1 mL	4.9 µL	0.65
LAMP	Betaine 5 M (molecular biology grade) Thermo Fisher Scientific	$41.65	10 mL	5.6 µL	0.02
LAMP	Primers (6 oligos; pricing basis) IDT DNA	$0.45/base	25 nmol scale	per LAMP stoichiometry	0.33 *(estimated)*
LAMP subtotal					1.36

Lysis	Proteinase K 20 mg/mL Thermo Fisher Scientific	$107.65	1.25 mL	10 µL	0.86
Lysis	Guanidine HCl (≥99%)	$324.00	500 g	0.191 g	0.12
Lysis	Triton X-100 MilliporeSigma	$61.70	100 mL	10 µL	0.01
Lysis	Tween-20 MilliporeSigma	$47.60	100 mL	1 µL	<0.01
Lysis	Tris base MilliporeSigma	$256.00	1 kg	0.0012 g	<0.01
Lysis subtotal					0.99
LFA	HybriDetect universal LFA kit (100 tests) Milenia Biotec	€250.00	100 tests	1 test	2.93
Chemistry + LFA subtotal					5.28

Table S3. Cartridge raw materials (example costing)

Cartridge item	Example price source	Pack price	Pack size	Assumed yield	Material cost per cartridge (USD)
PMMA/acrylic sheet (3 mm)	Etsy listing	$11.41	12"×19"	6 cartridges/sheet	1.90
3M 9474LE / 300LSE PSA (10 sheets)	Retail listing	$79.95	10 × (12"×12")	10 cartridges/sheet-equivalent	0.80
Transparency film (100 sheets)	Quartet/Apollo	$33.09	100 sheets	20 cartridges/box	0.17
Cartridge materials subtotal					2.87

Table S4. One-time device cost (heater + controller + sensor + PSU)

Device item	Example price source	Unit price	Qty	One-time cost (USD)
Minco polyimide heater HK6900 Minco	Minco catalog	$111.00	2	222.00
Minco CT325 controller (Pt100 input) Minco	Minco catalog	$187.00	1	187.00
Pt100 3-wire RTD sensor Evolution Sensors and Controls	EvoSensors	$50.00	1	50.00
12 V / 5 A PSU (example: Mean Well LRS-60-12 listing) eBay	Retail listing	$49.82	1	49.82
Estimated one-time device subtotal				508.82

Table S5. Comparison of HPV Detection Technologies (HPV16/18)

Method (Product)	Sample Type	Detection Time	Sensitivity	Specificity	Detection Method	LOD (copies/µL)	Multiplex	Reference
Integrated Microfluidic LAMP–LFA (This Work, 2025)	Cervical swab (direct)	~45 min (sample-to-answer)	96.8% (vs qPCR)	100%	Isothermal LAMP amplification	~10 copies/µL	Yes (HPV16 & 18)	*Manuscript draft*
Roche Cobas HPV Test (PCR)	Cervical (liquid cytology)	~3–4 hours (lab workflow)	~90% (≥CIN2)	~70%	Real-time PCR (TaqMan probes)	150–2400 copies/mL (genotype-dependent) (~0.15–2.4/µL)	Yes (14 hrHPV types; 16/18 genotyped)	14,15
Cepheid Xpert HPV (GeneXpert)	Cervical or vaginal swab	~60 min (cartridge)	92.3% (CIN2+, clinician)	53.3%	Automated PCR (nested real-time)	~2.9×10^3 IU/mL (HPV16) (~2.7×10^3 copies/mL)	Yes (HPV16, HPV18/45, others pooled)	15–17
Qiagen careHPV Test	Cervical or vaginal sample	~2.5 hours (batch)	86.4% (CIN2+, clinician)	80.4%	DNA Hybrid Capture + chemiluminescence	~1 pg HPV DNA (analytical; ~10^5 copies)	No (hrHPV pooled result)	17,18
Arbor Vita OncoE6™ Test	Cervical swab (protein)	~2 hours (rapid test)	54.5% (CIN2+)	98.4%	Lateral-flow immunoassay (E6 oncoprotein)	– (protein detection; no DNA LOD)	Yes (HPV16 & 18 E6 lines)	17
Fan et al. 2020 (Visual LAMP)	Cervical sample (DNA)	~65 min @ 63 °C	*"Comparable to qPCR"*	*High (validated vs PCR)*	LAMP (colorimetric, naked-eye)	~10–100 copies (per reaction)	No (separate 16/18 assays)	19,20
Wang et al. 2022 (Hydrogel LAMP)	Cervical sample (single-cell)	~30 min (rapid isothermal)	*"Comparable to qPCR"*	*High (vs qPCR)*	LAMP in hydrogel (in situ cell assay)	– (single infected cell detected)	No	21
Chen et al. 2022 (PCR–LFA)	Cervical sample (DNA)	~75 min	N/R (lab validation)	N/R	PCR amplification + LFA strip	~700 copies (per test)	Yes (HPV16 & 18)	22

Martínez-Fierro et al. 2025 (HDA Microfluidic)	Cervical swab (DNA)	<60 min (on-chip)	95.5%	100%	Helicase Dep. Amplification (isothermal)	~15 copies/reaction	Yes (HPV16 & 18)	[23]
Khamcharoen et al. 2023 (RPA Microfluidic)	Cervical DNA (HPV16)	~30 min (capillary chip)	N/R (limited testing)	N/R	Recombinase Pol. Amplification	~0.24 pg/µL (~30 copies/µL)	No	[24,25]
Zhao et al. 2023 (M-D3 CRISPR Device)	Cervical sample (DNA)	~30 min (on-chip)	92.3%	100%	RPA + CRISPR-Cas12a (droplet microfluidic)	~1 copy/reaction	Yes (HPV16 & 18)	[26]

The present LAMP–LFA microfluidic cartridge offers a fully *sample-to-answer* solution with integrated DNA extraction, amplification, and lateral-flow readout in ~45 minutes – faster than most lab tests (e.g. PCR) and without complex instruments. It achieves high diagnostic accuracy (≈97% sensitivity, 100% specificity) on cervical swabs, with a low DNA detection limit (~10 copies/µL). Compared to commercial assays, this device requires minimal equipment (no thermocycler or centrifuge) and is highly portable and affordable, making it ideal for point-of-care use in resource-limited settings. Notably, it simultaneously detects HPV16 and HPV18, providing multiplexed results similar to those of laboratory-based platforms, but at a fraction of the cost and infrastructure requirements. Overall, the present work stands out for its rapid, integrated POC operation and robust performance, combining the strengths of isothermal amplification and LFA in a field-deployable format.

Fabrication and Design of the Electronic Circuit and Heat Control Mechanism

All electronic components were securely mounted within a custom 3D-printed cradle, which was integrated into the fabricated structure. The system employs a straightforward and compact electronic design, avoiding unnecessary complexity. At its core, the temperature control mechanism consists of a digital temperature controller (CT325) and two flexible film heaters (10 mm × 30 mm, MINCO HK69002149) positioned on both the upper and lower sides of the amplification zone to ensure uniform heating. (Figure S1) A 12 V power adapter supplies power to both the temperature controller and the heating elements. Temperature sensing is achieved using a 3-wire Resistance Temperature Detector (RTD) wired for lead resistance compensation via the controller. The two common RTD wires, typically the same color, are connected to terminals 6 and 7, following standard wiring protocols, enabling precise temperature measurements. The

RTD sensor continuously monitors the system temperature and converts it into a voltage signal. This signal is then compared against the setpoint defined by an internal potentiometer. A solid-state output transistor is triggered if the measured temperature falls below the setpoint, activating the heaters. Once the temperature exceeds the setpoint, the transistor switches off, stopping the heating process. The operational status of the heater is indicated by a "Heat LED," which illuminates when the heater is active. This minimalistic and efficient setup ensures reliable thermal regulation with minimal electronic complexity, making it highly suitable for low-cost, portable diagnostic platforms.

Chitosan Functionalization of PMMA Microfluidic Channels

Microfluidic channel surfaces were functionalized with chitosan to impart pH-responsive nucleic acid capture capability via reversible electrostatic interactions. Prior to chitosan immobilization, the fabricated PMMA microfluidic chips were cleaned by sequential flushing with ethanol and deionized (DI) water and dried under a nitrogen stream. Because PMMA is intrinsically hydrophobic and chemically inert, surface activation was performed to introduce polar functional groups and improve coating stability.

Chemical activation of the PMMA microchannels was first carried out using alkaline hydrolysis (saponification). The channels were flushed with 1 M NaOH for 20 min, during which hydroxide ions attacked the ester side chains ($–COOCH_3$) of PMMA, converting them into surface-bound sodium carboxylate groups ($–COO^-Na^+$). The channels were subsequently rinsed thoroughly with DI water and flushed with 0.1 M HCl to protonate the carboxylate groups, yielding stable carboxylic acid functionalities (–COOH) on the channel walls. This treatment increased surface hydrophilicity and generated negatively charged sites suitable for polymer adsorption and covalent modification [1–3]. Following chemical activation, the PMMA microchannels were further treated with oxygen plasma to enhance surface oxidation and improve coating uniformity. Oxygen plasma generates reactive oxygen species that cleave C–C and C–H bonds at the polymer surface, leading to the formation of additional hydroxyl (–OH) and carboxyl (–COOH) groups. This dual activation strategy has been shown to significantly increase surface energy and promote stable biomolecule attachment on thermoplastic microfluidic substrates [4–6]. Low-molecular-weight chitosan (50–190 kDa, degree of deacetylation ≥75%) was dissolved at a concentration of 0.5–1.0% (w/v) in 1–2% (v/v) acetic acid under continuous stirring until a clear, homogeneous solution was obtained. The solution was filtered through a 0.22 µm syringe filter to remove undissolved particulates. The chitosan solution was introduced into the activated microchannels and incubated at room temperature for 30–60 min, allowing chitosan chains to adsorb onto the carboxylated PMMA surface through electrostatic interactions between protonated amine groups ($–NH_3^+$) and negatively charged carboxyl groups ($–COO^-$), as well as hydrogen bonding and van der Waals interactions [7–9]. Excess and loosely bound polymer were removed by flushing the channels with acetate buffer (pH 5.0), followed by gentle drying. To improve coating stability, the functionalized devices were thermally cured at 50–60 °C for 1 h. The resulting chitosan-functionalized microchannels exhibited

pronounced pH-dependent charge-switching behavior. Under acidic loading conditions (pH ≤ 5.5), the protonation of chitosan's primary amine groups imparted a net positive surface charge, enabling the efficient electrostatic capture of negatively charged DNA[10,11]. Following nucleic acid capture, the channels were flushed with deionized water to remove proteins, salts, and amplification inhibitors while retaining the bound nucleic acids on the chitosan-modified surface. Instead of performing a separate elution step, the amplification reagents were introduced directly into the microchannels, and nucleic acid amplification was carried out in situ on the same chip. This strategy eliminated the need for alkaline elution, minimized sample loss, and enabled a fully integrated, chaotrope-free sample-to-answer workflow compatible with on-chip nucleic acid amplification and detection [12,13].

Quantification and Calibration of Lateral Flow Assay (LFA) Strips Using ImageJ Analysis

To quantify the signal intensities of the test and control lines on the lateral flow assay (LFA) strips, images were first captured using a smartphone under consistent ambient lighting to ensure uniformity across all samples. These images were then analyzed using ImageJ software (National Institutes of Health). Each image was opened in ImageJ, and rectangular regions of interest (ROIs) were manually drawn to encompass the test line, control line, and an adjacent background area. This ensured standardized selection for all measurements. The selected image regions were then processed by inverting them to enhance contrast (via *Image* > *Adjust* > *Invert*) and subsequently converted to 32-bit grayscale format (*Image* > *Type* > *32-bit*) to enable more accurate intensity analysis. The average grayscale intensity of each ROI was measured using the "Measure" function (*Analyze* > *Measure*). This systematic image processing and analysis pipeline is illustrated in Figure S2, which summarizes the digital quantification methodology used for evaluating the LFA strip. To correct for background noise, the average intensity of the background ROI was subtracted from the intensity values of both the test and control lines. The corrected test line intensity was then divided by the corrected control line intensity to obtain the T/C (test/control) ratio for each strip. This T/C ratio served as the quantifiable metric corresponding to the concentration of the target analyte. For each target antigen, HPV-16 E6 or HPV-18 E6, a standard calibration curve was generated by plotting known antigen concentrations against their respective T/C ratios, as shown in Fig. S11.

Detection Pad Surface Modification

To improve fluid transport and ensure reliable lateral flow assay (LFA) performance, the detection pad region of the microfluidic cartridge was surface-modified to render it hydrophobic. This was achieved by applying a thin, uniform coating of a commercial transparent nail lacquer (e.g., *Sally Hansen Hard As Nails® Clear*), followed by gentle polishing to obtain a smooth surface finish. The hydrophobic modification reduced surface energy, preventing the nonspecific spreading or pooling of liquid at the detection interface. As a result, the eluted, amplified amplicons migrated smoothly and uniformly

across the lateral flow strip without lateral dispersion or stagnation. This simple surface treatment significantly improved the consistency of capillary-driven flow and signal clarity on the LFA, contributing to reproducible test-line development and a reliable endpoint readout. The use of readily available, low-cost, and transparent nail lacquer also aligns with the overall goal of developing a practical and scalable diagnostic platform suitable for point-of-care and low-resource settings.

Novelty and Key Innovations of the Integrated Microfluidic HPV Detection Platform

While loop-mediated isothermal amplification (LAMP) has been widely explored for HPV detection, the novelty of this work lies in the holistic integration of sample preparation, nucleic acid handling, amplification, and detection within a single disposable microfluidic cartridge, enabling a true *sample-to-answer* workflow. The platform uniquely incorporates a Zweifach–Fung bifurcation-based passive separation strategy for nucleic acid handling, eliminating the need for centrifugation, magnetic beads, or external pumping systems. A key innovation of this system is the integration of chitosan-based surface chemistry within the microfluidic channels, which enables pH-responsive, charge-switch-mediated nucleic acid capture and inhibitor removal. Chitosan-functionalized, chemically activated, and plasma-treated PMMA surfaces selectively bind negatively charged nucleic acids under acidic conditions, while allowing proteins, salts, and amplification inhibitors to be washed away, thereby improving compatibility with downstream on-chip amplification without requiring chaotropic agents or separate elution steps. The cartridge further integrates on-chip LAMP with an embedded lateral flow assay (LFA) readout, enabling direct visual detection and reducing the need for user intervention. Simultaneous detection of HPV-16 and HPV-18 within a single cartridge addresses the most clinically relevant high-risk human papillomavirus (HPV) genotypes. Finally, the use of a compact, low-power isothermal heating module supports portability and operation in low-resource settings. Collectively, the integration of passive microfluidics, chitosan-mediated nucleic acid handling, isothermal amplification, and on-chip lateral flow detection distinguishes this platform from existing LAMP-based HPV assays that rely on multiple off-chip or laboratory-dependent steps.

Cost and Practical Feasibility for Low-Resource Deployment

To assess the suitability of the proposed microfluidic LAMP–LFA platform for deployment in low-resource and decentralized clinical settings, a detailed cost analysis was performed covering assay reagents, consumables, and device fabrication. Based on current market pricing and laboratory-scale fabrication, the cost of LAMP reagents per test is approximately USD 1.3–1.6, while the room-temperature lysis buffer contributes an additional USD 0.9–1.0 per sample. The disposable multilayer microfluidic cartridge, fabricated from laser-cut PMMA, pressure-sensitive adhesive, and transparency films, has an estimated material cost of USD 2.5–3.0 per unit under small-batch production, with substantial scope for further reduction upon scale-up using injection molding or roll-to-roll lamination. Consequently, the total consumable cost per test is approximately

USD 5–6. The reusable heater and control module, comprising thin-film heaters, a digital temperature controller, an RTD sensor, and a power supply, has a one-time cost of approximately USD 450–550 and can be reused for several thousand assays, resulting in a negligible amortized per-test cost, and this information is added in the manuscript in *section 2.8*. In comparison with PCR-based HPV testing and commercial cartridge platforms, which typically require USD 15–50 per test along with sophisticated instrumentation and trained personnel, the proposed system offers a substantial reduction in cost while maintaining high diagnostic performance (96.8% sensitivity and 100% specificity) and a rapid sample-to-answer time of ~45 minutes. These features demonstrate the platform's strong potential for large-scale cervical cancer screening in resource-limited settings, including primary health centers, community clinics, and outreach screening programs.

1 A. C. Henry, T. J. Tutt, M. Galloway, Y. Y. Davidson, C. S. McWhorter, S. A. Soper and R. L. McCarley, *Anal. Chem.*, 2000, **72**, 5331–5337.

2 F. Fixe, M. Dufva, P. Telleman and C. B. V. Christensen, *Nucleic Acids Res.*, 2004, **32**, e9–e9.

3 C. R. Reedy, C. W. Price, J. Sniegowski, J. P. Ferrance, M. Begley and J. P. Landers, *Lab Chip*, 2011, **11**, 1603–1611.

4 S. Bhattacharya, A. Datta, J. M. Berg and S. Gangopadhyay, *J. microelectromechanical Syst.*, 2005, **14**, 590–597.

5 J. Zhou, A. V. Ellis and N. H. Voelcker, *Electrophoresis*, 2010, **31**, 2–16.

6 K. Ren, J. Zhou and H. Wu, *Acc. Chem. Res.*, 2013, **46**, 2396–2406.

7 E. L. Kendall, E. Wienhold and D. L. DeVoe, *Biomicrofluidics*.

8 K. A. Hagan, W. L. Meier, J. P. Ferrance and J. P. Landers, *Anal. Chem.*, 2009, **81**, 5249–5256.

9 N. Kumar, M. Kumari, D. Chander, S. Dogra, A. Chaubey and R. K. Arun, *Biomicrofluidics*.

10 W. Gan, Y. Gu, J. Han, C. X. Li, J. Sun and P. Liu, *Anal. Chem.*, 2017, **89**, 3568–3575.

11 J. Berger, M. Reist, J. M. Mayer, O. Felt and R. Gurny, *Eur. J. Pharm. Biopharm.*, 2004, **57**, 35–52.

12 X. Zhao, Y. Huang, X. Li, W. Yang, Y. Lv, W. Sun, J. Huang and S. Mi, *Talanta*,

2022, **250**, 123711.

13 T. S. Schlappi, S. E. McCalla, N. G. Schoepp and R. F. Ismagilov, *Anal. Chem.*, 2016, **88**, 7647–7653.

14 M. Saville, F. Sultana, M. J. Malloy, L. S. Velentzis, M. Caruana, E. L. O. Ip, M. H. T. Keung, K. Canfell, J. M. L. Brotherton and D. Hawkes, *J. Clin. Microbiol.*, 2019, **57**, 10–1128.

15 A. Rao, S. Young, H. Erlich, S. Boyle, M. Krevolin, R. Sun, R. Apple and C. Behrens, *J. Clin. Microbiol.*, 2013, **51**, 1478–1484.

16 *WHO Prequalification of In Vitro Diagnostics PUBLIC REPORT Product: Xpert HPV WHO reference number: PQDx 0268-070-00*, 2020.

17 R. Gupta, S. Singh and S. Gupta, *J. Public Health (Bangkok).*, 2025, **47**, e106–e115.

18 careHPV Test Kit, https://www.qiagen.com/gb/products/diagnostics-and-clinical-research/sexual-reproductive-health/cervical-cancer-screening/carehpv-test-kit.

19 L. Luo, K. Nie, M.-J. Yang, M. Wang, J. Li, C. Zhang, H.-T. Liu and X.-J. Ma, *J. Clin. Microbiol.*, 2011, **49**, 3545–3550.

20 Z. Fan, X. Feng, W. Zhang, N. Li, X. Zhang and J.-M. Lin, *Talanta*, 2020, **217**, 121015.

21 J. Wang, G. Jing, W. Huang, L. Xin, J. Du, X. Cai, Y. Xu, X. Lu and W. Chen, *Anal. Chem.*, 2022, **94**, 18083–18091.

22 Q. Chen, L. Yao, Q. Wu, J. Xu, C. Yan, C. Guo, C. Zhang, T. Xu, P. Qin and W. Chen, *Microchim. Acta*, 2022, **189**, 350.

23 E. González-González, E. A. Flores-Contreras, G. de J. Trujillo-Rodríguez, M. L. Jiménez-Martínez, I. P. Rodríguez-Sánchez, A. Ancer-Arellano, S. Alvarez-Cuevas, M. L. Martinez-Fierro, I. A. Marino-Martínez and I. Garza-Veloz, *Trop. Med. Infect. Dis.*, 2025, **10**, 272.

24 W. Khamcharoen, W. Siangproh, C. S. Henry, N. Sreamsukcharoenchai, P. Ratthawongjirakul and O. Chailapakul, *Sensors Actuators B Chem.*, 2024, **401**, 135016.

25 E. A. Flores-Contreras, E. González-González, G. de J. Trujillo-Rodríguez, I. P. Rodríguez-Sánchez, J. Ancer-Rodríguez, A. A. Pérez-Maya, S. Alvarez-Cuevas, M. L. Martinez-Fierro, I. A. Marino-Martínez and I. Garza-Veloz, *Pathogens*, 2024, **13**, 653.

26 Y. Zhao, D. Chen, Z. Xu, T. Li, J. Zhu, R. Hu, G. Xu, Y. Li, Y. Yang and M. Liu, *Anal. Chem.*, 2023, **95**, 3476–3485.